Cellular blueprint of healthy and diseased human epiglottis and subglottis—a study of the Canadian Airways Research (CARE) group

Peter Y. F. Zeng,[a,b,j,*] R. Jun Lin,[c,j,**] Kevin Fung,[a] Halema Khan,[a] Matthew J. Cecchini,[b] Elissa Woo,[b] Amanda Hu,[d] Jennifer Anderson,[c] Patrick MacInnis,[c] Laura Jarycki,[a] Amir Karimi,[a,b] Shengjie Ying,[a,b] MohdWessam Al Jawhri,[a,b] Sherman Lin,[a,b] Mushfiq Shaikh,[a,b,i] Harrison Pan,[a,b] Bryan Coburn,[e] Joe S. Mymryk,[a,f,g] Richard Inculet,[h] John W. Barrett,[a] and Anthony C. Nichols,[a,b,f,***] on behalf of the Canadian Airways Research Group of the Canadian Society of Otolaryngology Collaborative Research Initiative

[a]Department of Otolaryngology – Head & Neck Surgery, Western University, London, Ontario, Canada
[b]Department of Pathology and Laboratory Medicine, Western University, London, Ontario, Canada
[c]Department of Otolaryngology – Head & Neck Surgery, Temerty Faculty of Medicine, University of Toronto, Unity Health Toronto, St. Michael's Hospital, Toronto, Ontario, Canada
[d]Division of Otolaryngology, University of British Columbia, Vancouver, British Columbia, Canada
[e]Department of Medicine, University Health Network, University of Toronto, Toronto, Ontario, Canada
[f]Department of Oncology, Western University, London, Ontario, Canada
[g]Department of Microbiology & Immunology, Western University, London, Ontario, Canada
[h]Division of Thoracic Surgery, Western University, London, Ontario, Canada

eBioMedicine
2025;114: 105631
Published Online xxx
https://doi.org/10.1016/j.ebiom.2025.105631

Summary

Background The larynx consists of the supraglottis, glottis, and subglottis and each differ in tissue composition, lymphatic drainage, ability to counter infections, and response to injuries. However, the cellular mechanisms driving laryngeal homoeostasis remain largely unexplored. As a result, understanding disease pathogenesis within the larynx including idiopathic subglottic stenosis (iSGS) and intubation-related traumatic stenosis has been challenging. Here, we sought to characterise the cellular processes governing laryngeal health and disease.

Methods As part of the prospective Canadian Airways Research (CARE) iSGS study, we characterised 122,004 high-quality transcriptomes using single nucleus RNA-sequencing to profile 11 human epiglottis and 17 human subglottis biopsies across three different conditions: control, iSGS, and intubation-related traumatic stenosis to define cell populations and pathways associated with disease. We validated our results using cohort-level bulk transcriptomics using 114 human epiglottis and 121 human subglottis.

Findings We defined the single-cell taxonomy of the human subglottis and epiglottis using single-nucleus sequencing in both healthy and disease states. Mechanistically, we discovered the presence of unique epithelial and fibroblast progenitor subsets within the control subglottis but not within the anatomically adjacent epiglottis. The uncontrolled proliferation of these cellular subsets exhibited skewed sex hormone signalling and orchestrated a fibro-inflammatory cascade. We leveraged cohort-level bulk transcriptomics to define hallmarks of iSGS associated with disease covariates and introduced the first biomarker associated with recurrent relapse. Longitudinal sampling demonstrated that the subglottic microenvironment in patients with iSGS is changing dynamically with and without therapeutic intervention.

Interpretation Together, our data refines our understanding of laryngeal biology, nominates candidate compounds for iSGS treatment, and serves as a transformative platform for future clinical investigations to further precision laryngology.

*Corresponding author. Department of Otolaryngology - Head and Neck Surgery, Department of Pathology and Laboratory Medicine, Schulich School of Medicine and Dentistry, Western University, Victoria Hospital, London Health Science Centre, Room A4-431A, 800 Commissioners Road East, London, Ontario N6A 5W9, Canada.
**Corresponding author.
***Corresponding author. Department of Otolaryngology - Head and Neck Surgery, Schulich School of Medicine and Dentistry, Western University, Victoria Hospital, London Health Science Centre, Room B3-431A, 800 Commissioners Road East; London, Ontario N6A 5W9, Canada.
E-mail addresses: Peter.Zeng@lhsc.on.ca (P.Y.F. Zeng), RJun.lin@unityhealth.to (R.J. Lin), Anthony.Nichols@lhsc.on.ca (A.C. Nichols).
[i]Current address: School of Medicine, University of Texas-Rio Grande Valley, Edinburg, Texas, USA.
[j]These authors contributed equally.

Funding This study was funded by a grant from the American Laryngology Association (#1082), an Academic Medical Organisation of Southwestern Ontario innovation fund grant (INN21-016), grant support from the Departments of Otolaryngology—Head and Neck Surgery at University of Toronto, Canada and Western University, Canada. ACN was supported by the Wolfe Surgical Research Professorship in the Biology of Head and Neck Cancers Fund. PYFZ was supported by a Vanier Canada Graduate Scholarship and PSI Foundation fellowship.

Keywords: Idiopathic subglottic stenosis; Traumatic subglottic stenosis; Genomics; Transcriptomics; Biomarkers; Single-nucleus RNA-sequencing; Larynx

Research in context

Evidence before this study

The human laryngeal region is constantly exposed to a variety of physical, chemical, and inflammatory insults. However, our understanding of cellular processes that participate in the homoeostatic responses following these insults remains incomplete.

Added value of this study

Using large-scale single-nucleus RNA sequencing, we characterised epiglottis and subglottis tissue from patients in three different conditions–control, iSGS, and intubation-related traumatic stenosis–to define cell populations associated with disease pathogenesis and progression. Further integrative analyses of cohort-level bulk transcriptomics data identified tissue microenvironmental features associated with disease recurrence.

Implications of all the available evidence

Our study charts the cellular processes that underly the pathogenesis of subglottic stenoses and refine our understanding of homoeostatic processes in the laryngeal region in health and disease.

Introduction

Healthy human airway barrier function is maintained by carefully orchestrated and regulated injury responses that employ specialised epithelial, mesenchymal, endothelial, and immune cell subsets.[1,2] The human laryngeal region that lies at the intersection of upper and lower respiratory tract is structurally complex, functionally important, and constantly exposed to insults while playing key roles in phonation, breathing, swallowing, and protection from physical, chemical, and infectious insults. Anatomically, the larynx is divided into the supraglottis, glottis, and subglottis. Each have complex tissue niches with important differences in tissue composition, lymphatic drainage, and ability to counter infections and respond to injuries.[2–6] Nevertheless, despite the impressive knowledge base regarding the tissue and functional complexity of the larynx, we have limited understanding of the cellular homoeostasis and disease pathophysiology within the region. Furthermore, our understanding of processes governing laryngeal airway dynamics and remodelling responses to different nature of insults remains incomplete.

Past efforts to identify cellular subsets have been hindered by several factors. These include the lack of healthy subglottic tissue controls, limited cell sampling within modest cohort sizes, coverage of only a single anatomical region, and sampling bias from brushings that capture only superficial tissue layers. Additionally, the small sample sizes in previous studies restricted the ability to identify features associated with clinical outcomes, especially in a disease often treated heterogeneously with no standardised care. We recently reported a large-scale prospective cohort study of the disease subglottic stenosis.[7] Subglottic stenosis (SGS) encompasses a group of laryngeal conditions that may arise from trauma, such as prolonged intubation (traumatic SGS), autoimmune disease like granulomatous polyangiitis, or without any apparent cause (idiopathic).[8–12] The distinct aetiologies of SGS presents a valuable opportunity to shed light on tissue repair within the larynx following different initiation events.

In this study, we utilised paired biopsies of subglottic and supraglottic (epiglottic) regions of patients with idiopathic subglottic stenosis (iSGS), intubation-related traumatic SGS, and controls. These samples were prospectively collected as part of the Canadian Airways Research (CARE) group to investigate the cellular processes underlying the pathogenesis of these conditions. Using these data, we aimed to investigate the cellular populations linked to iSGS disease pathogenesis and their association with clinical outcomes. First, we constructed an integrated cellular atlas of the supraglottic and subglottic regions in control and diseased tissues. A large-scale integrated cellular atlas offers a unique opportunity to systematically identify the diverse cell types within the human larynx's supraglottic and subglottic regions. This comprehensive resource will serve to unravelling the cellular responses to intrinsic or physical injury. Using this dataset, we identified cell states associated with anatomical restriction and disease

pathophysiology in the two distinct types of SGS: traumatic and idiopathic. Finally, we introduced cellular niche archetypes of iSGS that correlate with specific clinical characteristics and patient outcomes. Our integrative study creates a platform to understand SGS and other airway disease, potentially enabling personalised precision laryngology.

Methods

Study population

Inclusion criteria for patients with SGS required a history of either idiopathic or traumatic SGS, being at least 18 years old, and the ability to provide consent. For the control group, inclusion criteria were: 1) female, 2) at least 18 years old, 3) self-identifying as Caucasian, 4) no prior history of SGS, head and neck cancer, or diseases affecting the subglottis, and 5) the ability to provide consent. These criteria for controls were designed to match the characteristics of patients with SGS. The controls for subglottic and epiglottic biopsy were recruited from patients presenting with conditions limited to the glottis (thus have healthy epiglottis and subglottis), such as laryngeal papillomatosis or vocal fold polyps.

Patients presenting with iSGS, traumatic SGS secondary to prolonged intubation, or controls were prospectively screened for study enrolment at tertiary laryngology clinics across each study site.

Fresh epiglottic and subglottic tissue samples were surgically obtained via biopsy and flash-frozen within 30 min of collection. Given the rarity of iSGS, no prior sample size calculation was performed. The sample size was determined based on the budget and availability of material. Thirty samples were selected to be prepared and sequenced, in which twenty-eight samples were successfully prepared and passed all quality control measures. Final data cut-off for clinical information follow-up was August 1st, 2023.

Ethics

The current case–control study received approval from the Research Ethics Board of all participating institutions (Western University [HSREB 115746], University of Toronto [#19-324], and University of British Columbia [H20-03149]). Written informed consent was obtained from all participants.

Single nucleus (sn) RNA-seq library preparation

Fresh epiglottic and subglottic samples were minced into 1–2 mm^3 pieces on dry ice using a chilled razor blade. The tissue was covered with lysis buffer and transferred to a tube to lyse on ice. The supernatant and pellet were dounced separately and transferred to chilled tubes. Douncing was complete when solution was milky. Nuclei viability was confirmed by SYBR staining using a Countess Cell Counter (Invitrogen Cat #C10283). Nuclei were collected by centrifugation (800×*g* for 10 min), repeated and then resuspended in 1 ml suspension buffer and passed through a 40 um Flowmi cell strainer. Nuclei were then loaded onto the Chromium single cell controller (10× Genomics) to construct a single nucleus 3' library. Sequencing was performed using NovaSeq 6000 sequencer.

snRNA-seq data quality control and preprocessing

snRNA-seq data were aligned and quantified using CellRanger (v6.0.2) against the reference human genome GRCh38 using the CellRanger count command. Empty droplets and ambient RNA were denoised using the CellBender[13] remove-background module. We than utilised scanpy (v1.9.3) for downstream quality control and processing. The quality of nuclei was assessed using the following criteria: 1) The number of detected genes was above 200; 2) the minimum number of transcript counts was above 500. We further removed nuclei whose total transcript count, genes detected, total mitochondrial transcript count, and mitochondrial transcript percentage were 5 median absolute deviation (MAD) above the median. We then logged and normalised transcripts counts per nucleus. We integrated the dataset across the two batches that they were processed in using harmonypy[14] with the run_harmony command. After batch correction, we did not observe obvious batch effects as most immune, cell, epithelial and stromal populations in different patients within the same tissue site mixed well. In total, after these stringent quality control measures our dataset contained 122,004 high quality nuclei.

Cell clustering, annotation, and pathway analysis

To identify cell states, we used the python scanpy (v1.9.3) package to identify highly variable genes (HVG) with a minimum mean of 0.0125, a max_mean of 3, and a minimum dispersion of 0.5 that resulted in 4694 highly-variables genes. Principal component analysis (PCA) was performed on the HVGs. Nearest neighbourhood graphs were generated using scanpy neighbours function. Clustering was performed using the leiden algorithm. Uniform Manifold Approximation and Projection (UMAP) was applied for dimensionality reduction.

We performed hierarchical annotations of the identified clusters. In the first level of cell annotations, we used well-characterised cellular markers to annotate cells as epithelial (*FXYD3, EPCAM, ELF3*), immune (*PTPRC, CD53, CORO1A*), stroma (*ECM2, OLFML1, SLIT2*), and endothelial (*CLDN5, ECSCR, CLEC14A*), which makes up cell type level 1. Full gene names used throughout the manuscript can be found in Supplementary Table S1. Tumour cells were identified using infercnvpy (v0.4.3). We then further annotated cell clusters using marker genes identified using the *scanpy rank_genes_groups* function hierarchically with

increasing precision until the finest level (cell type level 4). In total, we identified 8 endothelial populations (1 arterial, 2 venous, and 5 lymphatic), 25 epithelial populations (5 basal, 11 suprabasal, 2 ciliated, 2 club cell, 1 glandular, 1 goblet, 1 mucous, 1 myoepithelial, and 1 neuroendocrine populations), 11 stromal populations (8 fibroblast, 2 neuronal, and 1 smooth muscle cell populations), and 6 immune populations (3 lymphoid and 3 myeloid derived). PROGENy[15] as part of the decoupler-py (v1.5.0) through the multivariate linear model command run_mlm() was used to infer the activity of androgen and oestrogen pathways. The decoupler-py commands run_ora() was used to perform gene over representation analysis for snRNA-seq data.

Label transfer via logistic regression

CellTypist[16,17] v1.2.0 was used to train a logistic regression model from our dataset for label transfer using the celltypist.train function (tag-value pairs: use_SGD = True, feature_selection = True). Trained models from previously published datasets[18–21] were retrieved from (https://www.celltypist.org/models).

Tissue and disease type enrichment of cellular subsets

We utilised two different strategies to quantify and assess the cell clusters across tissue types (epiglottis or subglottis) and disease status (healthy control, trauma SGS, and iSGS). For each cellular subset in each major cellular type (immune, epithelial, stroma, and fibroblast), we calculated the $R_{o/e}$ value and compared the expected and observed number of cells for each cluster using the following formula as previously described:

$$R_{o/e} = \frac{Observed}{Expected}$$

The expected cell numbers for each combination of cell clusters and tissues are obtained from the χ^2 test. We further utilised a beta-binomial model in the sccomp package (v1.6.0)[22] to robustly perform variability analysis of the compositional data and statistical testing. Sccomp has been found to have improved performance over commonly used Dirichlet regression methods.

Trajectory analysis and RNA velocity

Cell trajectory were inferred using scFates[23] using principal tree inference settings and visualised using the scf.pl.trajectory command. The RNA velocity analysis was conducted using the scVelo package.[24] First, the spliced and unspliced counts were extracted from the preprocessed bam file using velocyto.[25] Then, scVelo's default preprocessing steps were applied, including filtering genes based on their velocity confidence. The velocities were estimated using the stochastic model provided by scVelo, which accounts for the transcriptional dynamics of splicing kinetics. The computed velocities were then projected onto a PCA embedding for visualisation, facilitating the interpretation of cellular trajectories and potential fate decisions.

Cell–cell ligand-receptor interaction network analysis

Given the frequent discrepancy of output of individual tools, we adopted a consensus approach to analyse cell–cell ligand-receptor interactions, implemented using the liana-py package.[26] For cellular subsets within each disease tissue (iSGS subglottic, control subglottis, etc.), we scored ligand-receptor pairs using eight different methods including CellPhoneDB, Connectome, log2FC, NATMI, SingleCellSignalR, CellChat, and GeoMetric Mean. We limited the cell subsets to those that are present in each disease and tissue by restricting analysis to the only interactions of cell subsets with $R_{o/e}$ greater than 0.5 in the specific disease tissue. Highly ranked interactions were then scored using rank and aggregation of interactions from all methods. We defined putative high–quality interactions as those that fit all of the following criteria: 1) CellPhone *P*-value less than 0.001; 2) CellChat *P*-value less than 0.001; 3) scaled weight greater than 1; 4) aggregate specificity weight less than 0.001. We plotted the cell–cell interaction by calculating the interaction strength between each cell subset by summing the strength between identified significant putative ligrand–receptor interactions. We then applied the Fruchterman-Reingold layout algorithm to the network defined using the strength as the edge weight, and cell type as nodes using the igraph (v1.6.0) package. Node output strength was also computed using igraph package.

SCENIC regulon analysis

To identify activated regulons, we utilised the SCENIC package using the python implementation pySCENIC, as previously described.[27] We estimated gene–gene co-expression relationships between transcription factors and their potential targets using the multiprocessing version of the *grn* command. The *aucell* command was used to estimate the regulon activity for each cell.

SUBglottiS gEne subType (SUBSET) iSGS subtypes

To derive potential cellular composition relationships between cell subsets in iSGS subglottic samples, we first derived consensus cell modules using consensus clustering implemented using the ConsensusClusterPlus package. We utilised estimated cell abundance from CibersortX using Pearson correlation as the distance metric and Ward Linkage with 1000 repetitions and 0.8 proportions of items per sample. We calculated the cumulative distribution function of the consensus matrix for each k subgroups to identify the optimal number of cluster numbers k at which the cumulative distribution function plateaus. For the number of cell clusters, the optimal k identified is 5, which we labelled as cell

modules C-M1 to C-M5. Using this information, we then calculated the total abundance of cell types in each cell modules C-M1 to C-M5 for each sample and performed hierarchical clustering through hclust to derive cellular composition subtypes of iSGS, which we label SUBglottiS gEne subtype (SUBSET). The optimum number of clusters for hierarchical clustering was identified using silhouette statistic. The SUBSET subtypes are labelled as SUBSET1—SUBSET4.

Statistics

All statistical analysis were conducted using R (v4.2.1) or python (v3.8.7). Cox-proportional hazards models were used for survival analyses. Specifically, the Cox models were specified with 1) the time of biopsy as the start of the survival interval; 2) the next surgical dilation or intra-office steroid injection as event and not adjusting for any covariates as there are no robust factors associated with time to next intervention. Patients were censored at the time of their last known follow-up if no event had occurred. The study cut-off date was at the study cut-off date August 1st, 2023. The proportional hazards assumption was checked using Schoenfeld residual test, with a significance level of $P < 0.05$ as evidence against the assumption. Wilcoxon test, Fisher's exact test, and Poisson regression were performed using the packages rstatix, or stats. The Poisson regression model was specified using the dependent variable is the number of events within the follow-up time and SUBSET as independent variable and BMI, age at diagnosis, smoking, antiacids use, and Cotton-Myers grade as covariates using a log-link function. Only one Poisson model was performed. Overdispersion was checked by calculating the dispersion parameter and overdispersion was not detected. Confidence interval for Poisson regression were estimated using robust sandwich estimators. Unless stated otherwise in the figure legend or text, multiple comparison was corrected using the Benjamini-Hochberg procedure, as previously described.[28] For single cell analyses, Benjamini-Hochberg procedure multiple testing adjustments for statistical tests were determined by the number of the transcripts and cell types as specified using scanpy.

Role of funders

The funders of the current study had no role in the design, data collection, data analyses, interpretation, or writing of report.

Results

Single cell blueprint of epiglottic and subglottic tissue in healthy and diseased states

To investigate the cellular underpinnings of subglottic stenoses, we performed single-nucleus RNA sequencing (snRNA-seq) of 17 subglottis and 11 epiglottis samples collected prospectively from 18 patients (10 patients with iSGS, 5 controls, and 3 trauma patients with SGS). Out of the 28 samples subjected to snRNA-seq, there were 10 epiglottis–subglottis pairs from the same patient. After stringent quality control and filtering of the snRNA-seq data (see Methods), we obtained 122,004 high-quality transcriptomes (Fig. 1a). There were minimal batch effects, with most cell populations represented by cells from multiple patients (Supplementary Figure S1a). To define major populations and subpopulations of cell states, we performed graph-based clustering which revealed a total of 50 clusters followed by expert iterative manual annotation (see Methods). In total, our cell atlas revealed 25 epithelial

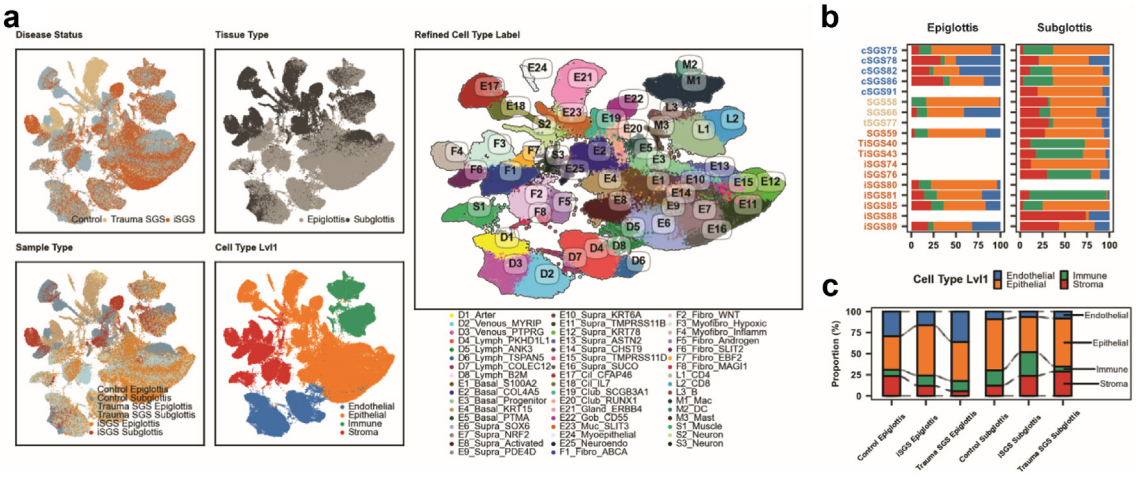

Fig. 1: **A single cell atlas of the healthy and diseased epiglottis and subglottis.** **a)** UMAP visualisation of cell states and annotated with disease status, tissue type, sample type, coarse cell type (level 1) labels, and finely annotated (level 4) cell type labels. **b)** Distribution of coarse cell type annotations by patient (cell type level 1). **c)** Proportion of profiled cells by sample type (disease status and tissue type).

(E) cell clusters, 11 stromal (F) clusters, 8 endothelial (D) clusters, and 6 immune cell clusters (Fig. 1a–c, Supplementary Figure S1a–c). We explored the similarity and divergence of cell subsets to previous published single-cell/nuclei atlases of the respiratory system in other healthy and diseased contexts encompassing data from the lung, bronchi, trachea, and nasopharynx.[18–21] Using logistic regression-based label transfer[16] (see Methods), we found that most observed immune and endothelial populations within the subglottis and epiglottis found in our atlas were also present in other atlases. On the other hand, many of the epithelial and fibroblast cell subsets exhibited tissue restriction within the subglottis and epiglottis, and were not present in other healthy or fibrotic cell atlases. This highlights important tissue-specific differences within the laryngeal region compared to other respiratory regions (Supplementary Figure S2a–d). Therefore, our data not only captured both previously described immune, epithelial, stromal, and fibroblast cells within the subglottis and epiglottis, but also revealed previously undescribed cell states that may contribute to unique disease pathologies in the subglottis.

Anatomically distinct, disease-associated epithelial populations in the epiglottis and subglottis

Airway epithelium rapidly responds to injury to prevent barrier loss.[29–31] Progenitor populations, such as basal cells, can differentiate into secretory, glandular, and ciliated cells to resolve damage. Given the close proximity of the subglottis to the epiglottis, their exposure to similar external insults and pathogens, and the lack of molecular alterations in the epiglottis region in patients with extensive fibrotic disease in iSGS, we hypothesised that intrinsic differences in cell type composition predispose the subglottis to fibrosis. As many epithelial cell types in our cell atlas are distinct from other respiratory cell atlases (Supplementary Figure S2), we first focused on the epithelial cell subsets within the subglottis and epiglottis. The 25 identified epithelial cell subsets (Fig. 2a) are defined by distinct transcriptional markers (Supplementary Figure S3a) and activated transcriptional pathways (Supplementary Figure S3b). We examined the enrichment of individual epithelial cell subsets across disease-tissue using two orthogonal modelling approaches. Within the epiglottis, $R_{o/e}$ enrichment analysis and compositional analyses (see Methods) suggest that there are minimal cellular compositional differences between the iSGS epiglottic tissue and control epiglottic tissue (Fig. 2a, Supplementary Table S2a). Further, we detected no difference in the estimated abundance of each of the epithelial cell subsets between the control and iSGS epiglottis in our bulk RNA-seq cohort (Fig. 2c top panel, Wilcoxon rank-sum FDR P-value > 0.05).

We next turned our attention to the subglottis. E23 *SLIT3* mucinous cells and E24 myoepithelial cells are enriched in both the trauma SGS epiglottis and subglottis (Fig. 2b), suggesting similar trauma-driven aetiology across these two anatomic sites from prolonged intubation. Further, we identified enrichment of several cell subsets (Fig. 2b) in iSGS subglottic tissue compared to control subglottis, including E10 suprabasal cells, E20 *RUNX1*+ cells, and E22 goblet cells. The E22 *CD55*+ goblet cells are almost exclusively found in the iSGS subglottic region, but not detected in either control or trauma SGS. Despite inter-patient heterogeneity for bulk RNA-seq, we observed largely similar enrichment patterns in estimated epithelial cell subsets in the subglottis at the cohort level (Fig. 2c). Collectively, these results underscore the unique compositional changes in epithelial cell states within the subglottis of iSGS and trauma patients with SGS. This data also highlights the remarkable anatomical tissue restriction pathologies to the subglottis is observed only in iSGS, but not trauma SGS.

Inflammatory, androgen-skewed secretory cell subsets reinforce the iSGS local subglottic niche

We molecularly dissected the epithelial cell subsets that are specific to the subglottis and either enriched or depleted in iSGS or trauma SGS in both the single cell and bulk RNA-seq datasets following the two distinct modes of injury initiation—likely microenvironmental (iSGS) and physical (trauma SGS). Gene set enrichment analysis found that iSGS-subglottic specific cells are marked by expression of a high abundance of transcripts related to androgen response (Fig. 2d, Supplementary Figure S3b). We formally inferred downstream oestrogen and androgen pathway activity in each of the epithelial subsets using PROGENy[15] and identified that E22 goblets cells have increased androgen pathway responsiveness and lower oestrogen responsiveness compared to other epithelial subsets (Fig. 2e). Furthermore, the E22 goblet cells express a higher abundance of gene sets pertinent to complement activation, JAK-STAT signalling, and inflammatory pathways such as TNF-alpha (Supplementary Figure S3b).

To discern the transcriptional trajectories of the epithelial populations within the subglottis, we utilised two orthogonal methods to study cellular fate. Trajectory analysis[23] and RNA velocity[24] (Fig. 2f–h) suggest that basal cell populations shared across control and diseased subglottic tissue could give rise to club cells and mucous producing cells. In contrast, basal cells in control subglottis differentiate into suprabasal cells and E19 *SCGB3A1* club cells that are *MUC5B*+ (Fig. 2f–h). Basal cells in iSGS give rise to E20 *RUNX1* club cells or further convert into E22 CD55+ goblet cells, which are marked by increased response to androgen and decreased response to oestrogen in iSGS (Fig. 2h), in contrast with the E21 glandular cells enriched in trauma SGS that maintain a high response of both the androgen and oestrogen pathways. The E22 CD55+ goblet cells that express high amounts of *MUC5AC* and *SPDEF*

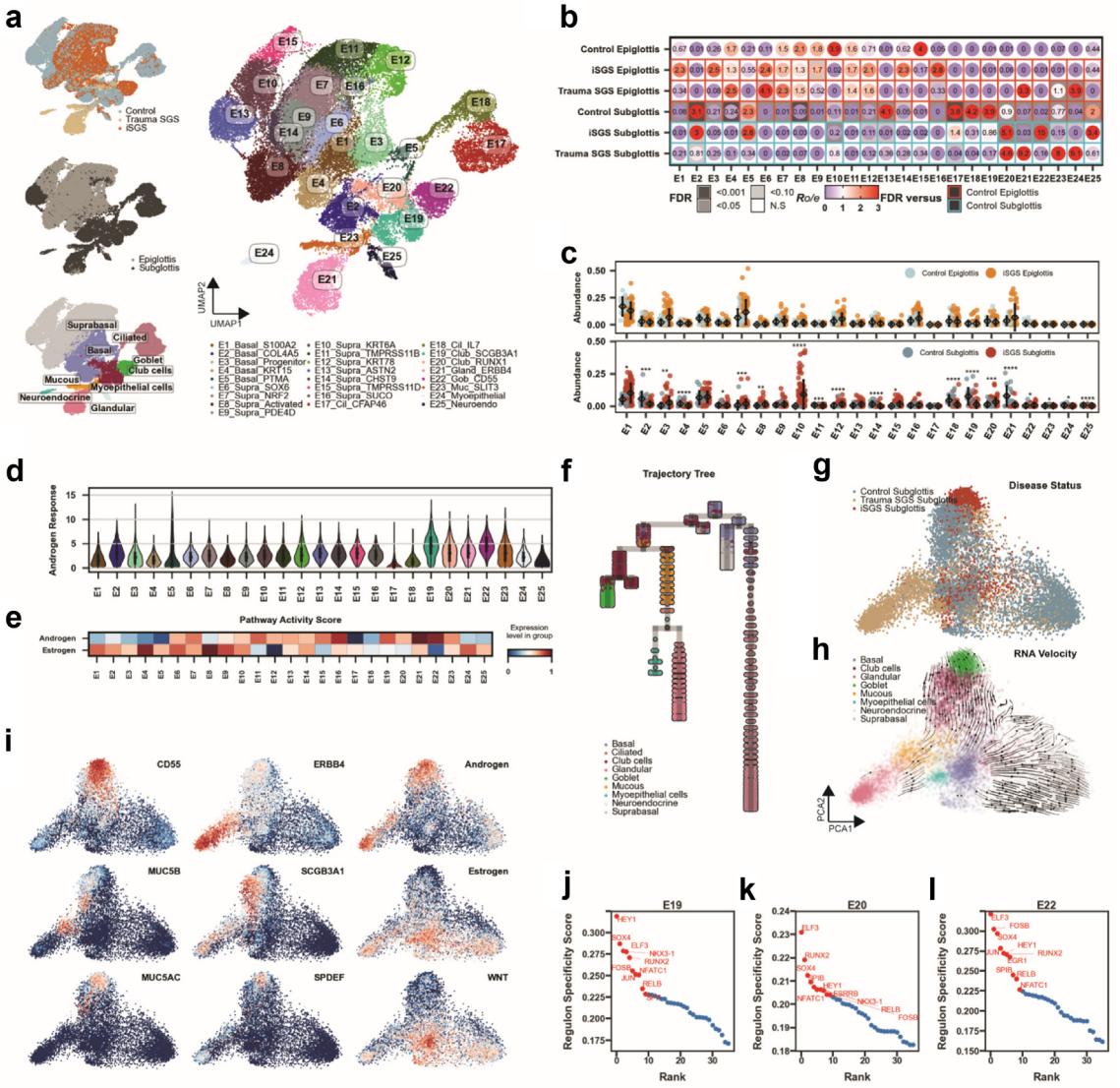

Fig. 2: **Epithelial heterogeneity and dysfunction in subglottic stenoses**. **a)** UMAP visualisation of 25 epithelial cell states and annotated with disease status, tissue type, sample type, level 3 cell type labels, and finely annotated (level 4) cell type labels. **b)** Sample type tissue prevalence estimated by $R_{o/e}$ score. FDR derived from statistical compositional difference testing using sccomp package, corrected with Benjamini-Hochberg procedure. Statistical comparisons of iSGS epiglottis, trauma SGS epiglottis, and control subglottis made against control epiglottis, while iSGS subglottis and trauma SGS subglottis were compared against control subglottis. **c)** Abundance of each estimated of epithelial cell type in the epiglottis (top) and subglottis (bottom) from bulk RNA-seq using CIBERSORT. FDR from Benjamini-Hochberg adjusted Wilcoxon test. *: FDR <0.05, **: FDR <0.01, ***: FDR <0.001, ****: FDR <0.0001. **d)** Gene ontology enrichment value for androgen response in each epithelial subset. **e)** Pathway output activity of androgen and oestrogen inferred using PROGENy, normalised between groups. **f)** Inferred developmental trajectory of epithelial cells from the subglottis using pseudotime using scFate package, colour by their cell type level 3 annotations. **g** and **h)** PCA-representation of the developmental trajectory of epithelial cells from the subglottis inferred using RNA velocity and coloured using either the disease status (**g**) or cell type level 3 annotation (**h**). **i)** PCA visualisation of transcript abundance of *CD55*, *MUC5AC*, *SCGB3A1*, *MUC5B*, *ERBB4*, and *SPDEF*, along with PROGENy inferred pathway output activity score of androgen, oestrogen, and WNT-signalling. **j–l)** Scatter plot showing the specificity scores of regulons in E19 (**j**), E20 (**k**), and E22 (**l**) cell populations. The top 10 regulons are highlighted.

(Fig. 2i) were located at the end of the velocity and show decreased pathway activity of WNT-signalling, thereby inferred as the terminal state. The depletion of *MUC5B* + *SCGB3A1*+ cells concur with our bulk RNA-seq data, where the abundance of *SCGB3A1* and *MUC5B* was significantly decreased in iSGS subglottis compared to control subglottis (FDR *P*-value < 0.0001, Wilcoxon test, Supplementary Figure S3c).

Intriguingly, gene regulatory programs inferred using pySCENIC(27) (Methods) identified regulons in E20 and E22 controlled by the *ELF3* encoded transcriptional factor that is necessary for airway club cells to resolve epithelial injury (Fig. 2j–l, Supplementary Figure S3d).[32] On the other hand, the *HEY1* encoded transcription factor was specific to the E19 club cells, which are abundant in the control subglottis but depleted in both iSGS and trauma SGS. HEY1 is a mediator of NOTCH signalling that regulates airway epithelial progenitor stem cell fate decision[33] by serving as an androgen receptor (AR) co-repressor and controlling the expression of genes down stream of AR.[34] All together, these findings imply that secretory cell subsets in the subglottis undergo a profound and conserved transcriptional response that leads to differential activity of sex hormone pathways in response to distinct disease aetiologies. Taken together, our data proposes a model where a yet-unidentified disease-initiating event in the subglottis of iSGS induces dysregulated hormonal signalling in the epithelial cell subsets. These sustained hormonal dysregulation drives epithelial differentiation of club cells to inflammatory goblet cells, which are hyper-responsive to androgen. Critically, the enrichment of these androgen-responsive cell subsets within the subglottic region of iSGS may thus explain the near exclusivity of the disease to premenopausal females.

Origin, divergence, and function of subglottic fibroblast populations

We next examined mesenchymal subsets, focussing on fibroblasts as they coordinate response to injuries and orchestrate tissue repair.[35] Within the control and diseased epiglottis and subglottis, we discovered eight distinct fibroblast populations (Fig. 3a) that exhibit unique tissue and disease distribution (Fig. 3b, Supplementary Figure S4a) and are characterised by distinctive transcriptional programs (Supplementary Figure S1b). The remarkable divergence in tissue distribution between these fibroblast subsets is highlighted by the near exclusivity of F4 inflammatory myofibroblasts in the subglottis tissue of iSGS (Fig. 3b, Supplementary Table S2b), that is further supported within our bulk RNA-seq dataset (Fig. 3c, Wilcoxon test FDR $P < 0.0001$). Furthermore, in trauma SGS, fibroblast populations differ both between the epiglottis and subglottis compared to that of controls, but also with those found in the iSGS, indicative of differential fibrotic response leading to similar pathologies (Fig. 3b). F3 fibroblasts enriched in trauma SGS have high expression of hypoxic genes (Supplementary Figure S4b), possibly reflecting the long period of intubation these patients experienced.

We then sought to understand the differences between the fibroblasts within the control subglottis. The majority of fibroblast populations in the control subglottis consists of F3 myofibroblasts and F6 fibroblasts (Fig. 3b–e) that express high abundance of *SLIT2*, encoding a secreted cell migration factor. These cells protect against fibrosis in healthy tissues by inhibiting myofibroblast differentiation and tissue fibrosis.[36] The F6 fibroblasts also express high amounts of *AXIN2*, a WNT-pathway regulator, which correlates with a population of myofibrogenic progenitor cells in airways that readily differentiate into myofibroblasts. Fascinatingly, a similar subset *AXIN2*+ cells are found in the rare genetic disease pulmonary lymphangioleiomyomatosis (LAM),[37] a respiratory disease that shares many clinical features with iSGS—near exclusivity to females of childbearing age–and the *AXIN2*+ myofibrogenic progenitor cells that generate pathologically deleterious myofibroblasts after injury in idiopathic pulmonary fibrosis.[29]

RNA velocity analysis suggests that F1 and F6 fibroblasts (Fig. 3d), depleted in both trauma SGS and iSGS, expand divergently into F4 and F3 myofibroblasts in iSGS and trauma SGS respectively. The acquisition of these myofibroblast cell states is accompanied by the expression of *TGFβ*, *VEGF*, and myogenic transcriptional programs. In addition, the F3 and F4 myofibroblasts are accompanied by acquisition of unique marker genes such as *COL1A1* in F4, and *CREB5* and *SOX6* in F3 (Fig. 3f). The progenitor state of F6 fibroblasts is further supported by gene regulatory network analysis (Fig. 3f), with increased expression of stemness-related transcriptional factors *SOX17* and *NFATC4*.[38–40] Furthermore, both F4 (Fig. 3g) and F6 (Fig. 3f) fibroblasts have high activity of *RELB* regulon, which is crucial for NF-κB-mediated inflammation along with enrichment of JAK-STAT and interferon response, which was not observed in fibroblast populations enriched in the control epiglottis (Supplementary Figure S4b). Collectively, our data suggest that the human control subglottis contains a group of fibroblast populations that is primed for inflammation and fibrotic repair. These cells respond to injury through differentiation into myofibroblasts, which are absent within the epiglottis and could explain why stenosis is restricted solely to the subglottic region. Similarly, these F3, F4 and F6 cells are absent in normal lung tissue (Supplementary Figure S2a and b) but are present in idiopathic pulmonary fibrosis tissue samples (Supplementary Figure S2c and d).

Rational prioritisation of candidate targeted therapeutics to reverse iSGS fibrosis

We next utilised a perturbation-transcriptional response connectivity database to link candidate compounds to revert the fibrotic change from F4 to F6 (see Methods). The class of compounds with the highest similarity with expression program that reverses the gene expression change from F4 to F6 include glucocorticoid receptor agonists, TGF-beta receptor inhibitors, and heat shock protein inhibitors (Fig. 3h, Supplementary Table S3).

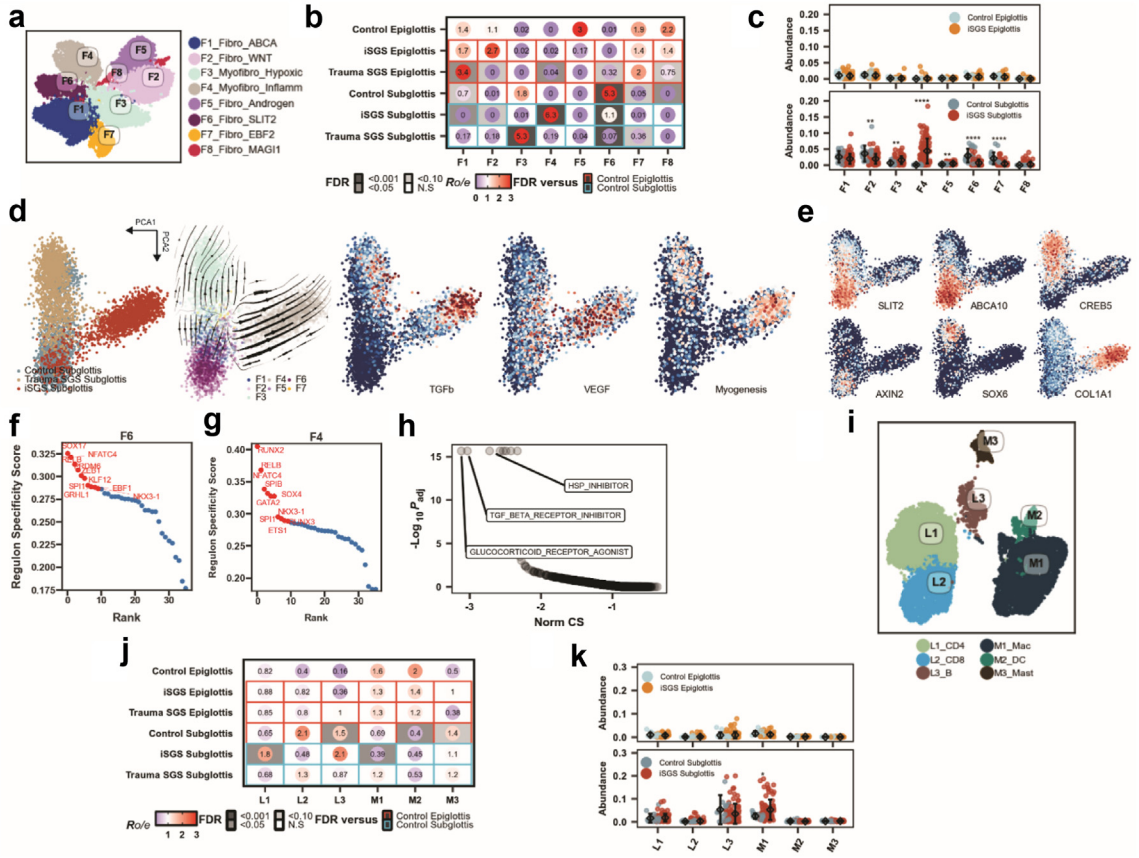

Fig. 3: **Distinctive fibroblast populations within the subglottis primed for expansion**. **a)** UMAP visualisation of eight fibroblast cell states. **b)** Sample type tissue prevalence estimated by $R_{o/e}$ score. FDR from sccomp scores, corrected with Benjamini-Hochberg procedure. Statistical comparisons of iSGS epiglottis, trauma SGS epiglottis, and control subglottis made against control epiglottis, while iSGS subglottis and trauma SGS subglottis were compared against control subglottis. **c)** Abundance of each estimated fibroblast cell states in the epiglottis (top) and subglottis (bottom). FDR from Benjamini-Hochberg adjusted Wilcoxon test. **: FDR <0.01, ***: FDR <0.001, ****: FDR <0.0001. **d)** Inferred developmental trajectory of RNA velocity of fibroblast found in the control subglottis, trauma SGS subglottis, and iSGS subglottis. Pathways are coloured by activity of TGFβ, VEGF, and myogenesis pathways. **e)** PCA visualisation of transcript abundance of *SLIT2*, *ABCA10*, *CREB5*, *AXIN2*, *SOX6*, and *COL1A1*. **f, g)** Scatter plot showing the regulon specificity scores of transcription factor in F6 (**F**) and F4 (**g**) fibroblasts. Top 10 regulons are highlighted. **h)** Connectivity Map analysis of potential therapeutics to reverse gene expression of F4 fibroblasts. Norm connectivity score (CS) and adjusted *P-values* from ConnectivityMap query module. **i)** UMAP visualisation of immune cell subset. **j)** Sample type tissue prevalence estimated by $R_{o/e}$ score. FDR from compositional analysis performed using the sccomp package, corrected with Benjamini-Hochberg procedure. Statistical comparisons of iSGS epiglottis, trauma SGS epiglottis, and control subglottis made against control epiglottis, while iSGS subglottis and trauma SGS subglottis were compared against control subglottis. **k)** Abundance of each estimated immune cell states in the epiglottis (top) and subglottis (bottom). FDR from Benjamini-Hochberg adjusted Wilcoxon test. *: FDR <0.05.

These classes of compounds have all been widely investigated in mitigating and reversing fibrosis of other respiratory diseases[41–43] such as idiopathic pulmonary fibrosis and thus warrants further clinical investigation in the disease context of iSGS. The potential of these compounds to change clinical progression of iSGS fibrosis is strengthened by the observation that glucocorticoid steroid injections are widely used in the clinic and operating room to delay the need for further surgical interventions.[44–47] Future studies will be needed to study the comparative efficacy of these agents in the context of iSGS.

A chorus of cell interactions defines cellular ecosystem, plasticity, and rewiring to sustain tissue remodelling in iSGS

In our single cell dataset, we detected a lower number of macrophages and increased abundance of L1 CD4 T cells in the iSGS subglottis compared to control subglottis (Fig. 3i and j). However, using the larger bulk RNA-seq cohort level we identified an overall increase in the abundance of M1 macrophages (Fig. 3k, Supplementary Table S2c) and did not identify differences between lymphocyte populations (L1 CD4 T cells, L2 CD8 T cells, or L3 B cells, Fig. 3k). These data

suggest significant disease heterogeneity in the immune cell populations within the microenvironment both in control and iSGS subglottis tissue. We next turned to eight identified endothelial populations (Supplementary Figure S5a and b) within our snRNA-seq dataset, and found that iSGS exhibited distinct venous and lymphatic cell abundances compared to control subglottis (Supplementary Figure S5c and d).

To gain insights into the crosstalk between the cell populations during homoeostasis and disease, we interrogated global cell–cell interactions in healthy and diseased epiglottis and subglottis using a stringent consensus model implemented through LIANA that aggregates the results of eight state-of-the-art ligand-receptor inference tools[26] (see Methods). We began by focussing on the control epiglottis, where we identified putative receptor–ligand interactions between cellular subsets in the epiglottis from control, trauma, and patients with iSGS (Supplementary Figure S6).

In control epiglottis (Supplementary Figure S6a) and similarly undiseased iSGS epiglottis (Supplementary Figure S6b) endothelial and fibroblasts populations form the central nodes of the signalling network. In contrast, epithelial subsets E24 myoepithelial cells, E21 glandular ERBB4, and E23 mucinous SLIT3 cell populations form the strongest interactions in trauma SGS epiglottis (Supplementary Figure S6c). Similarly in traumatic SGS subglottis (Supplementary Figure S6f), E24 were found to be the central node of the network, implicating these cells in orchestrating the inflammatory response following long-term intubation. Finally, we found that the iSGS subglottis interaction network (Supplementary Figure S6e) consisted of fewer nodes compared to both the control subglottis (Supplementary Figure S6d) and trauma SGS subglottis (Supplementary Figure S6f). In particular, the iSGS subglottis network is dominated by E5 basal cells, which secrete large amount of growth factors that coordinate tissue repair (Supplementary Figure S6e), such as *MIF*, a key factor in promoting wound healing and tissue repair.[48,49] Among the other top interactions in iSGS were between *CD55* in E22 Goblet cells and *ADGRE2* on mast cells (Supplementary Figure S6g), which play vital roles in potentiating inflammation and autoimmunity.[50–53] Taken together, our data suggests that iSGS and trauma SGS both exhibit distinct rewiring of cell signalling that contributes to the two distinct types of fibrosis.

Tissue microenvironment niche and plasticity in iSGS

Cells within human tissues form complex niches that dynamically interact. To understand cellular heterogeneity in iSGS at a cohort-level, we examined co-enrichment patterns of cells from estimated cellular abundance in the subglottis inferred using bulk RNA-seq to define the cellular ecosystem archetypes of iSGS. Consensus clustering revealed five stable cellular modules (C-M1 to C-M5) in iSGS subglottis samples that have inter-correlated abundance patterns (Fig. 4a, Supplementary Figure S7a, Methods). The C-M1 module consisted of cell subsets such as F4 Myofibroblasts, L1 CD4 T cells, L3 B cells, and M1 Macrophages. The co-existence of these cell subsets suggests a coordinated and sustained fibroinflammatory response within the subglottis. The C-M 2 module consists of E11 suprabasal, D5 lymphatic, and E24 myoepithelial cells, while the C-M 3 module is characterised by L2 CD8 T-cells and suprabasal cells. C-M4 consists of basal cells, and club cell-derived cell subsets (e.g. E20 club *RUNX1* and E22 goblet cells). Finally, C-M5 consisted of E19 club cells and E21 glandular cells. Using these cell modules (C-M1—C-M5), we assigned patients into one of four subglottic subtypes based on the abundance of cells within each of the coordinated cell module using a cluster approach. We named this classification system SUBSET (**SUB**glotti**S** g**E**ne sub**T**ype, Fig. 4b, see Methods). SUBSET1 subglottis consisted mainly of cells from the C-M3 cell module that are CD8 T-cells and suprabasal cells, with lower proportion of C-M4 and C-M1 module. SUBSET2 subglottis was enriched with C-M1, C-M3, and C-M4 cell modules, suggestive of both secretory epithelial cells and fibroinflammatory cell populations. Cells from SUBSET3 consisted of a large proportion C1 cell subsets with also smaller proportion of C-M3, C-M4, and C-M5 modules, while C-M1 and C-M2 constitutes the majority of samples in SUBSET4.

We next examined the association between SUBSET with the clinical trajectory of patients. SUBSET was not associated with clinical parameters at the time of tissue sample acquisition such Cotton-Myers score ($P = 0.94$, Fisher's exact test, Supplementary Figure S7c). However, compared to SUBSET1, patients with SUBSET3 or SUBSET4 subglottis were associated with the increased rate of intervention (dilation or steroid injection) during follow up (Fig. 4c, multivariate Poisson regression with follow-up time as offset), a measure of long-term disease severity. These results suggest that the SUBSET classification (Fig. 4d) is predictive of the intervention rate over time of patients with iSGS, with SUBSET3 and SUBSET4 patients experiencing more events compared to SUBSET1 patients and thus more aggressive long-term disease.

We further studied microenvironmental plasticity within the iSGS subglottis in the 11 patients with multiple biopsies available and characterised these using bulk RNA-seq. Only three of eleven patients (27%) exhibited concordant SUBSET types between at least two time points (Fig. 4e), suggesting that the molecular microenvironment of iSGS can evolve spontaneously or following therapeutic intervention through either dilation or steroid injection. The evolving subglottic microenvironment in iSGS may pose challenges for the usage of targeted therapies or monoclonal antibodies

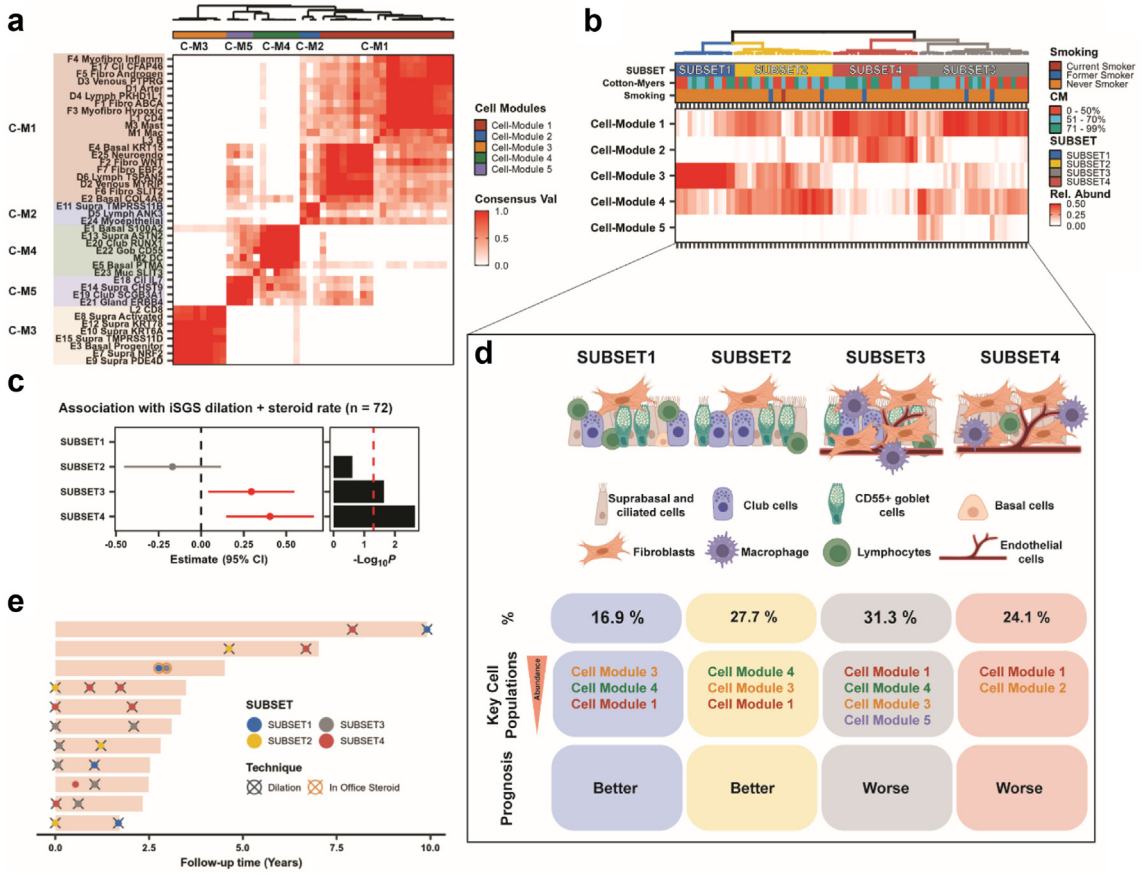

Fig. 4: **Cellular and molecular classification of iSGS. a)** Cell type modules identified using consensus clustering of cell type abundance (n = 83). Only cell types with $R_{o/e}$ above 0.01 in at least one of control, iSGS, or trauma SGS subglottis is included. **b)** SUBglottiS gEne subtype (SUBSET) microenvironment archetypes identified using clustering of identified relative abundance. **c)** Association between each SUBSET cluster and total number of interventions (n = 72). Only the first sample for patients with multiple samples were considered. Estimate, 95% confidence interval, and *P*-values from Poisson regression. **d)** Summary of patients stratified by SUBSET. **e)** SUBSET changes with or without treatment demonstrating microenvironment plasticity patients with iSGS with multiple samples.

towards a specific cell population, and future work will be needed to understand the interplay between these variables and clinical outcomes.

Discussion

The low incidence of iSGS has precluded detailed molecular characterisation at a cohort level. In this study, single cell profiling of a prospectively collected cohort allowed us to decipher the single-cell taxonomy of the human subglottis and epiglottis in both healthy and diseased states. Moreover, we developed a biomarker associated with recurrent relapse in iSGS. Currently laryngologists primarily employ a treat and observe approach for iSGS. Pending further validation, the SUBSET classifier may facilitate the identification of patients with severe disease and optimise therapy for these high-risk patients.

Our findings have important clinical and mechanistic implications. Biologically, our data reveal the presence of epithelial and fibroblast progenitor subsets within the control subglottis, which are less abundant in the adjacent epiglottis. Dysregulation in the differentiation and proliferation of these progenitor cell subsets may initiate a fibroinflammatory cascade following injury or as a response to other, yet unidentified, stimuli. Further, we demonstrate that contrary to a previous hypothesis of generalised airway abnormalities,[54] the cellular population in the epiglottic tissue of patients with iSGS largely resembles that of controls. Moreover, we identify a notable enrichment of androgen-responsive and oestrogen unresponsive club-cell-derived subsets in iSGS, setting it apart from trauma-induced SGS. Given the hypothesised influence of hormonal signalling in iSGS, especially given its prevalence in women of child-bearing age, these club-cell-derived

subsets are likely significant contributors to disease pathogenesis. Collectively, our results support the theory that sex hormones may play a contributory, if not driving, role in the development of iSGS.

Clinically, our work revealed significant heterogeneity between the subglottic tissue of patients with iSGS in subglottic tissue among patients with iSGS through standardised prospective sample collection. Longitudinal sampling indicates dynamic changes in the subglottic microenvironment in iSGS, potentially explaining variability in recurrence intervals observed among patients. These microenvironment changes could profoundly influence the design of clinical investigations using targeted therapies or immunotherapeutic approaches aimed at specific cell population. Nevertheless, given that the biopsy only covered limited tissue, future studies will be needed to better characterise these identified changes and their implications for iSGS management.

The current study has several limitations. Firstly, due to cost constraints and challenges in obtaining sufficiently small biopsies from this anatomically difficult location, we were only able to profile a subset of patients using single-cell profiling. Nevertheless, we have used a larger bulk RNA-sequencing cohort to validate our single cell findings. As the cost of single cell profiling decreases, we anticipate expanding our dataset further. Combining expanded single cell transcriptomic data along with genetic information may enable identification of cell-type specific expression QTLs that may be associated with disease.[55,56] Furthermore, due to the inaccessibility of the anatomic site, the biopsies are inherently small, and sampling bias cannot be ruled out. Future research should aim to expand our findings by exploring intra-patient heterogeneity across different treatments, locations, and time points. Lastly, while we have gained potential insights into cellular subsets, molecular pathways, and candidate therapeutics, our findings will require validation in animal models or prospective clinical trials to draw definitive conclusions.

In summary, we provide a cellular blueprint of the larynx, which bridges the upper and lower respiratory tract. Our multi-scale datasets offer significant insights into the heterogeneity and complexity of subglottic stenoses. Importantly, our research infrastructure could be leveraged to investigate other poorly understood diseases of the laryngeal region, advancing precision laryngology and potentially improving patient outcomes.

Contributors

P.Y.F.Z., R.J.L, and A.C.N. analysed the data. R.J.L, P.Y.F.Z, H.K, and A.C.N conceptualized the study. R.J.L, K.F, H.K, M.J.C, E.W, A.H, J.A, P.M, A.K, S.Y, M.A.J, S.L, L.J, M.S, H.P, B.C, J.S.M, R. I, J.W.B, and A.C.N collected research data and provided study resources for the study. A.C.N. and R.J.L provided funding for the study. R.J.L, A.C.N and P.Y.F.Z. supervised the study. All authors contributed to data interpretation, writing, and editing of the manuscript. R.J.L and P.Y.F.Z contributed equally to the study and declare that either author may list their name first. All authors read and approve the final version of the manuscript. Members of the study consortium participated in the study in at least one of the following ways: 1) participated in the design and analysis of the study; 2) collected patient sample; 3) collected patient clinical datal; 4) participated in the experimental process.

Data sharing statement

All generated single nuclei data are available at EGA (accession code: EGAD50000001279). Upon reasonable request, deidentified code used in the analyses can be shared with other researchers by communicating to the corresponding authors.

Declaration of interests

A.C.N has research funding from Novartis Canada, Merck Canada, LabCorp, and Droplet Biosciences for studies that are unrelated to the submitted work. He has equity from and is a consultant for NEED Inc. M.J.C has research funding from Astra Zeneca, Merck and Pfizer, he has received payment for speaker honorarium and/or served on advisory boards for Eli Lilly Merck, Astra Zeneca, and Amgen. M.J.C has equity from and is a consultant for NEED Inc. A.H has consulted for Merck Inc and serves on the advisory board for Pentax Inc, both unrelated to the current study. P.Y.F.Z, J.W.B, J.S.M, and A.C.N hold patents for transcriptional biomarker in head and neck cancer, unrelated to this work. R.J.L, K.F, H.K, E.W, J.A, P.M, L.J, A.K, S.Y, M.A.J, S.L, M.S, H.P, B.C, and R. I have no conflicts of interest to declare.

Acknowledgements

We acknowledge all patients, family members, and caregivers who participated in the current study. We would like to thank Drs. Danielle Macneil and Adrian Mendez collected specimens (<5) for this study. Ms. Sabrina Rashid and Ms. Silkan Bains helped with specimen handling and transportations at Unity Health Toronto, St. Michael's Hospital. Ms. Lama Elkadri helped with sample transportation and data collection.

Appendix A. Supplementary data

Supplementary data related to this article can be found at https://doi.org/10.1016/j.ebiom.2025.105631.

References

1 Hewitt RJ, Lloyd CM. Regulation of immune responses by the airway epithelial cell landscape. *Nat Rev Immunol*. 2021;21(6):347–362.
2 Zepp JA, Morrisey EE. Cellular crosstalk in the development and regeneration of the respiratory system. *Nat Rev Mol Cell Biol*. 2019;20(9):551–566.
3 Reynolds SD, Reynolds PR, Pryhuber GS, Finder JD, Stripp BR. Secretoglobins SCGB3A1 and SCGB3A2 define secretory cell subsets in mouse and human airways. *Am J Respir Crit Care Med*. 2002;166(11):1498–1509.
4 Zuo WL, Shenoy SA, Li S, et al. Ontogeny and biology of human small airway epithelial club cells. *Am J Respir Crit Care Med*. 2018;198(11):1375–1388.
5 Hillel AT, Samad I, Ma G, et al. Dysregulated macrophages are present in Bleomycin-induced murine Laryngotracheal stenosis. *Otolaryngol Head Neck Surg*. 2015;153(2):244–250.
6 Riede T, Stein A, Baab KL, Hoxworth JM. Post-pubertal developmental trajectories of laryngeal shape and size in humans. *Sci Rep*. 2023;13(1):7673.
7 Lin RJ, Zeng PYF, Fung K, et al. Cohort-level clinical trajectory and molecular landscape of idiopathic subglottic stenosis for precision laryngology – a study of the Canadian Airways Research (CARE) group. *eBioMedicine*. 2025. In Press.
8 Axtell AL, Mathisen DJ. Idiopathic subglottic stenosis: techniques and results. *Ann Cardiothorac Surg*. 2018;7(2):299–305.
9 Valdez TA, Shapshay SM. Idiopathic subglottic stenosis revisited. *Ann Otol Rhinol Laryngol*. 2002;111(8):690–695.
10 Park SS, Streitz JM Jr, Rebeiz EE, Shapshay SM. Idiopathic subglottic stenosis. *Arch Otolaryngol Head Neck Surg*. 1995;121(8):894–897.
11 Aravena C, Almeida FA, Mukhopadhyay S, et al. Idiopathic subglottic stenosis: a review. *J Thorac Dis*. 2020;12(3):1100–1111.
12 Brandenburg JH. Idiopathic subglottic stenosis. *Trans Am Acad Ophthalmol Otolaryngol*. 1972;76(5):1402–1406.

13 Fleming SJ, Chaffin MD, Arduini A, et al. Unsupervised removal of systematic background noise from droplet-based single-cell experiments using CellBender. *Nat Methods*. 2023;20(9):1323–1335.
14 Korsunsky I, Millard N, Fan J, et al. Fast, sensitive and accurate integration of single-cell data with Harmony. *Nat Methods*. 2019;16(12):1289–1296.
15 Schubert M, Klinger B, Klunemann M, et al. Perturbation-response genes reveal signaling footprints in cancer gene expression. *Nat Commun*. 2018;9(1):20.
16 Dominguez Conde C, Xu C, Jarvis LB, et al. Cross-tissue immune cell analysis reveals tissue-specific features in humans. *Science*. 2022;376(6594):eabl5197.
17 Xu C, Prete M, Webb S, et al. Automatic cell type harmonization and integration across human cell atlas datasets. *Cell*. 2023;186(26):5876–5891.e20.
18 Madissoon E, Oliver AJ, Kleshchevnikov V, et al. A spatially resolved atlas of the human lung characterizes a gland-associated immune niche. *Nat Genet*. 2023;55(1):66–77.
19 Habermann AC, Gutierrez AJ, Bui LT, et al. Single-cell RNA sequencing reveals profibrotic roles of distinct epithelial and mesenchymal lineages in pulmonary fibrosis. *Sci Adv*. 2020;6(28):eaba1972.
20 Adams TS, Schupp JC, Poli S, et al. Single-cell RNA-seq reveals ectopic and aberrant lung-resident cell populations in idiopathic pulmonary fibrosis. *Sci Adv*. 2020;6(28):eaba1983.
21 Sikkema L, Ramirez-Suastegui C, Strobl DC, et al. An integrated cell atlas of the lung in health and disease. *Nat Med*. 2023;29(6):1563–1577.
22 Mangiola S, Roth-Schulze AJ, Trussart M, et al. sccomp: robust differential composition and variability analysis for single-cell data. *Proc Natl Acad Sci U S A*. 2023;120(33):e2203828120.
23 Faure L, Soldatov R, Kharchenko PV, Adameyko I. scFates: a scalable python package for advanced pseudotime and bifurcation analysis from single-cell data. *Bioinformatics*. 2023;39(1):btac746.
24 Bergen V, Lange M, Peidli S, Wolf FA, Theis FJ. Generalizing RNA velocity to transient cell states through dynamical modeling. *Nat Biotechnol*. 2020;38(12):1408–1414.
25 La Manno G, Soldatov R, Zeisel A, et al. RNA velocity of single cells. *Nature*. 2018;560(7719):494–498.
26 Dimitrov D, Turei D, Garrido-Rodriguez M, et al. Comparison of methods and resources for cell-cell communication inference from single-cell RNA-Seq data. *Nat Commun*. 2022;13(1):3224.
27 Van de Sande B, Flerin C, Davie K, et al. A scalable SCENIC workflow for single-cell gene regulatory network analysis. *Nat Protoc*. 2020;15(7):2247–2276.
28 Benjamini Y, Hochberg Y. Controlling the false discovery rate: a practical and powerful approach to multiple testing. *J Roy Stat Soc B*. 1995;57(1):289–300.
29 Zepp JA, Zacharias WJ, Frank DB, et al. Distinct mesenchymal lineages and niches promote epithelial self-renewal and Myofibrogenesis in the lung. *Cell*. 2017;170(6):1134–1148.e10.
30 Lynch TJ, Anderson PJ, Rotti PG, et al. Submucosal gland myoepithelial cells are reserve stem cells that can regenerate mouse tracheal epithelium. *Cell Stem Cell*. 2018;22(5):653–667.e5.
31 Tata A, Kobayashi Y, Chow RD, et al. Myoepithelial cells of submucosal glands can function as reserve stem cells to regenerate airways after injury. *Cell Stem Cell*. 2018;22(5):668–683.e6.
32 Oliver JR, Kushwah R, Wu J, et al. Elf3 plays a role in regulating bronchiolar epithelial repair kinetics following Clara cell-specific injury. *Lab Invest*. 2011;91(10):1514–1529.
33 Byrnes LE, Deleon R, Reiter JF, Choksi SP. *Opposing transcription factors MYCL and HEY1 mediate the Notch-dependent airway stem cell fate decision*. 2022.
34 Belandia B, Powell SM, Garcia-Pedrero JM, Walker MM, Bevan CL, Parker MG. Hey1, a mediator of notch signaling, is an androgen receptor corepressor. *Mol Cell Biol*. 2005;25(4):1425–1436.
35 Plikus MV, Wang X, Sinha S, et al. Fibroblasts: origins, definitions, and functions in health and disease. *Cell*. 2021;184(15):3852–3872.
36 Pilling D, Zheng Z, Vakil V, Gomer RH. Fibroblasts secrete Slit2 to inhibit fibrocyte differentiation and fibrosis. *Proc Natl Acad Sci U S A*. 2014;111(51):18291–18296.
37 Obraztsova K, Basil MC, Rue R, et al. mTORC1 activation in lung mesenchyme drives sex- and age-dependent pulmonary structure and function decline. *Nat Commun*. 2020;11(1):5640.
38 Wang P, Rodriguez RT, Wang J, Ghodasara A, Kim SK. Targeting SOX17 in human embryonic stem cells creates unique strategies for isolating and analyzing developing endoderm. *Cell Stem Cell*. 2011;8(3):335–346.
39 Zhang L, Jambusaria A, Hong Z, et al. SOX17 regulates conversion of human fibroblasts into endothelial cells and erythroblasts by dedifferentiation into CD34(+) progenitor cells. *Circulation*. 2017;135(25):2505–2523.
40 Herum KM, Lunde IG, Skrbic B, et al. Syndecan-4 signaling via NFAT regulates extracellular matrix production and cardiac myofibroblast differentiation in response to mechanical stress. *J Mol Cell Cardiol*. 2013;54:73–81.
41 King TE Jr, Pardo A, Selman M. Idiopathic pulmonary fibrosis. *Lancet*. 2011;378(9807):1949–1961.
42 Martinez FJ, Collard HR, Pardo A, et al. Idiopathic pulmonary fibrosis. *Nat Rev Dis Primers*. 2017;3(1):17074.
43 Mora AL, Rojas M, Pardo A, Selman M. Emerging therapies for idiopathic pulmonary fibrosis, a progressive age-related disease. *Nat Rev Drug Discov*. 2017;16(11):755–772.
44 Gelbard A, Anderson C, Berry LD, et al. Comparative treatment outcomes for patients with idiopathic subglottic stenosis. *JAMA Otolaryngol Head Neck Surg*. 2020;146(1):20–29.
45 Gelbard A, Donovan DT, Ongkasuwan J, et al. Disease homogeneity and treatment heterogeneity in idiopathic subglottic stenosis. *Laryngoscope*. 2016;126(6):1390–1396.
46 Maldonado F, Loiselle A, Depew ZS, et al. Idiopathic subglottic stenosis: an evolving therapeutic algorithm. *Laryngoscope*. 2014;124(2):498–503.
47 Nouraei SA, Sandhu GS. Outcome of a multimodality approach to the management of idiopathic subglottic stenosis. *Laryngoscope*. 2013;123(10):2474–2484.
48 Dunbar H, Hawthorne IJ, Tunstead C, Armstrong ME, Donnelly SC, English K. Blockade of MIF biological activity ameliorates house dust mite-induced allergic airway inflammation in humanized MIF mice. *FASEB J*. 2023;37(8):e23072.
49 Takahashi K, Koga K, Linge HM, et al. Macrophage CD74 contributes to MIF-induced pulmonary inflammation. *Respir Res*. 2009;10(1):33.
50 Yona S, Lin HH, Dri P, et al. Ligation of the adhesion-GPCR EMR2 regulates human neutrophil function. *FASEB J*. 2008;22(3):741–751.
51 Gray JX, Haino M, Roth MJ, et al. CD97 is a processed, seven-transmembrane, heterodimeric receptor associated with inflammation. *J Immunol*. 1996;157(12):5438–5447.
52 Huang YS, Chiang NY, Hu CH, et al. Activation of myeloid cell-specific adhesion class G protein-coupled receptor EMR2 via ligation-induced translocation and interaction of receptor subunits in lipid raft microdomains. *Mol Cell Biol*. 2012;32(8):1408–1420.
53 Boyden SE, Desai A, Cruse G, et al. Vibratory Urticaria associated with a missense variant in ADGRE2. *N Engl J Med*. 2016;374(7):656–663.
54 Damrose EJ. On the development of idiopathic subglottic stenosis. *Med Hypotheses*. 2008;71(1):122–125.
55 Perez RK, Gordon MG, Subramaniam M, et al. Single-cell RNA-seq reveals cell type-specific molecular and genetic associations to lupus. *Science*. 2022;376(6589):eabf1970.
56 Yazar S, Alquicira-Hernandez J, Wing K, et al. Single-cell eQTL mapping identifies cell type-specific genetic control of autoimmune disease. *Science*. 2022;376(6589):eabf3041.